University of Massachusetts Amherst

From the SelectedWorks of Jianhua Yang

Spring May 5, 2009

The mechanism of electroforming of metal oxide memristive switches

Jianhua Yang, *University of Massachusetts - Amherst*
Feng Miao
Matthew Pickett
Douglas Ohlberg
Duncan Stewart, et al.

Available at: https://works.bepress.com/jianhua-yang/2/

The mechanism of electroforming of metal oxide memristive switches

J Joshua Yang, F e n g M i a o , Matthew D Pickett,
Douglas A A Ohlberg, Duncan R Stewart, Chun Ning Lau and R
Stanley Williams

Abstract
Metal and semiconductor oxides are ubiquitous electronic materials. Normally insulating, oxides can change behavior under high electric fields—through 'electroforming' or 'breakdown'—critically affecting CMOS (complementary metal–oxide–semiconductor) logic, DRAM (dynamic random access memory) and flash memory, and tunnel barrier oxides. An initial irreversible electroforming process has been invariably required for obtaining metal oxide resistance switches, which may open urgently needed new avenues for advanced computer memory and logic circuits including ultra-dense non-volatile random access memory (NVRAM) and adaptive neuromorphic logic circuits. This electrical switching arises from the coupled motion of electrons *and* ions within the oxide material, as one of the first recognized examples of a memristor (memory–resistor) device, the fourth fundamental passive circuit element originally predicted in 1971 by Chua. A lack of device repeatability has limited technological implementation of oxide switches, however. Here we explain the nature of the oxide electroforming as an electro-reduction and vacancy creation process caused by high electric fields and enhanced by electrical Joule heating with direct experimental evidence. Oxygen vacancies are created and drift towards the cathode, forming localized conducting channels in the oxide. Simultaneously, O^{2-} ions drift towards the anode where they evolve O_2 gas, causing physical deformation of the junction. The problematic gas eruption and physical deformation are mitigated by shrinking to the nanoscale and controlling the electroforming voltage polarity. Better yet, electroforming problems can be largely eliminated by engineering the device structure to remove 'bulk' oxide effects in favor of interface-controlled electronic switching.

1. Introduction

Electronic switching in nanoscale metal/titanium oxide/metal devices [1, 2] has recently been reported and linked to the memristor circuit element theory originally predicted in 1971 by Chua [3]. A simplified memristor device physics model [1] matched the experimental behavior [2] of nano-crossbar Pt/TiO_2/Pt devices. Resistive switching in metal oxides has in fact seen more than four decades of scientific research [4–15], motivated in large part by that prospect of a fast and high density NVRAM technology [16–23]. The continuous resistance change exhibited by oxide switches also appears to meet analog switch requirements for neuromorphic computing [24–26]. Despite this promise, answers to some key questions have remained elusive for the devices due to the lack of solid experimental evidence and the metal oxide technology has not yet matured.

The least understood, and most problematic, step in the operation of these metal oxide switches is typically the 'electroforming' process, a one-time application of high voltage or current that produces a significant change of electronic conductivity [27–30]. Subsequent to this change the devices operate as tunable resistance switches, but with a wide variance of properties dependent on the details of the electroforming. This variance is an Achilles' heel limiting the adoption of metal oxide switches in computing circuits. In this report we explain the electroforming mechanism for a bipolar metal/oxide/metal switch by identifying the active species responsible for the irreversible change, the behavior under bipolar forming voltages, and the relation to subsequent electrical switching. Based on these insights, we postulate and then demonstrate a method to eliminate the electroforming process altogether. This understanding yields new control and repeatability to promise improved engineering of the switches for future nanoscale integrated circuits.

The least understood, and most problematic, step in the operation of these metal oxide switches is typically the 'electroforming' process, a one-time application of high voltage or current that produces a significant change of electronic conductivity [27–30]. Subsequent to this change the devices operate as tunable resistance switches, but with a wide variance of properties dependent on the details of the electroforming. This variance is an Achilles' heel limiting the adoption of metal oxide switches in computing circuits. In this report we explain the electroforming mechanism for a bipolar metal/oxide/metal switch by identifying the active species responsible for the irreversible change, the behavior under bipolar forming voltages, and the relation to subsequent electrical switching. Based on these insights, we postulate and then demonstrate a method to eliminate the electroforming process altogether. This understanding yields new control and repeatability to promise improved engineering of the switches for future nanoscale integrated circuits.

2. Experimental section

A typical device structure is Si/SiO_x/Ti 5 nm/Pt 15 nm/TiO_2 25–50 nm/Pt 30 nm, as schematically shown in upper-left inset to figure 1(a). All the metal layers, including Pt and Ti, were deposited via e-beam evaporation with the substrate at the ambient temperature. The TiO_2 layers were deposited by sputtering from a polycrystalline rutile TiO_2 target with the Ar pressure of ~1.5 mTorr and the substrate temperature of 275 ± 25 °C. The Ti (1.5 nm adhesion layer) + Pt (8 nm) electrode used for the 50 nm × 50 nm nano-junctions was patterned by ultraviolet-nanoimprint lithography. The Ti (5 nm adhesion layer) + Pt (15 nm for BE and 30 nm for TE) electrodes used for the micro-junctions (5 μm × 5 μm) were fabricated using a metal shadow mask. Some samples adopted a highly reduced TiO_{2-x} layer, which was deposited at 0.3 nm s^{-1} by reactive-sputtering from a Ti target with a 93% Ar and 7% O_2 gas mixture. A HP 4156 semiconductor parameter analyzer was used for the electrical characterization with the 4-probe DC measurement method. All voltages were applied to the top electrode (TE); the bottom electrodes (BE) of the junctions were electrically grounded during all measurements. All electrical measurements were done in air at 300 K. The plan-view TEM sample (figure S1 (available at stacks.iop.org/Nano/20/215201)) was made by depositing 50 nm TiO_2 film on top of a single crystal NaCl and then putting the NaCl crystal with the film into de-ionized water to peel the film off as a TEM sample. The AFM images were processed with WSxM [31].

3. Results and discussion

The idealized electrical behavior of a memristive oxide switch is shown in figure 1(a). Repeatable ON/OFF switching follows a 'bowtie' or 'figure-8' shaped current–voltage I–V curve (blue). This repeatable switching is only arrived at, however, after an electroforming step of high positive voltage (red) or high negative voltage (green) changes the device from a virgin near-insulating state into an ON/OFF switching state. As shown in figure 1(a), opposite polarities of forming voltage and current typically produce opposite initial states of the switch. Usually, an external voltage sweep from 0 up to −20 V (negative forming) or +10 V (positive forming) is applied for the electroforming and the device could be formed before reaching these maximum voltages. Once the device is formed at a certain voltage, e.g. −12 V, during the voltage sweep from 0 to −20 V, a jump at −12 V towards a higher current and a lower voltage is observed in the I–V curve, indicating the occurrence of the forming at this voltage. After forming, the device resistance decreases by several orders of magnitude and the majority drop of the applied external voltage shifts from the device to the wires accordingly. After a negative voltage sweep (green curve in figure 1(a)), the device is formed in the ON state while a positive voltage sweep (red curve) forms the device in the OFF state with the typical ON/OFF resistances shown in figures 1(b) and (c) for nano- and micro-devices, respectively. After electroforming, both nanoscale and micron scale devices show repeatable non-volatile bipolar switching up to 10^4 cycles. These devices are switched ON by a negative voltage and switched OFF by a positive voltage on the top electrodes. Polarity of switching is usually controlled by the asymmetry of the interfaces as fabricated; for all reported devices the top interface is Schottky-like and the bottom interface is ohmic-like [2] (figure 1(a), inset).

Figure 1(d) presents atomic force microscopy (AFM) images for nano-devices with a 50 nm thick TiO_2 insulator sandwiched between 50 nm wide Pt nanowire electrodes, as fabricated by nanoimprint lithography (NIL) [32, 33]. The TiO_2 is a sputter-deposited amorphous or nanocrystalline thin film (see supplemental information figure S1 (available at stacks.iop.org/Nano/20/215201) for x-ray diffraction and transmission electron microscopy data; see [2] for additional related materials properties). No noticeable difference in the switching characteristics has been observed between amorphous and nanocrystalline TiO_2. Among these 1 × 17 nano-junctions, the 2nd and the 15th junctions (indicated by blue arrows) have been electrically formed and switched, including more than 50 cycles for the 2nd junction. An AFM cross-section profile is also shown. For the nano-junctions, no topographic difference can be detected between the formed devices and the virgin devices.

In striking contrast, clear physical deformation appeared for the micro-devices after electroforming. Figures 1(e) and (f) show AFM images of a micro-device before and after a one-time negative voltage electrical forming process with a voltage sweep from 0 to −14 V. A large dome-like physical deformation has appeared along the edge of the bottom electrode (figure 1(f)). Dimensions of the dome in cross-section show a diameter of about 1 μm and a height of about 50 nm. An eruption-like feature is visible on the top of the dome. This device consisted of 5 μm wide, 15 nm thick top and 30 nm thick bottom Pt electrodes separated by a 50 nm thick blanket TiO_2 layer.

Physical deformations have been reported to accompany electroforming in metal/oxide/metal structures since the 1960s, however the causes are still controversial and have been attributed to a number of mechanisms including electrode

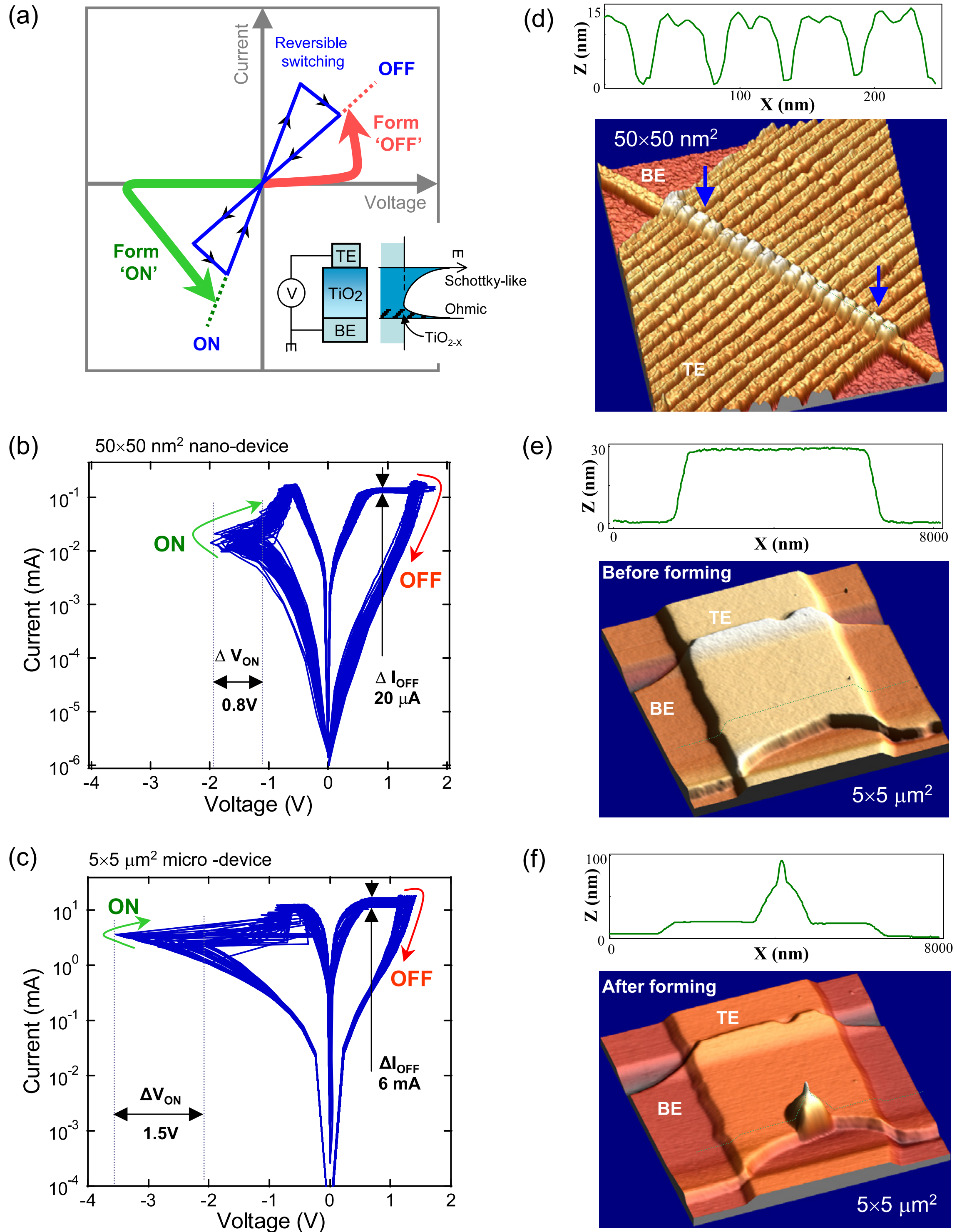

Figure 1. Electrical switching and forming for nano- and micro-devices. Voltages are applied to the top electrode (TE); the bottom electrode (BE) is grounded for all measurements in this report. (a) Schematic of the forming step and subsequent bipolar reversible switching. The device can be irreversibly formed by either a positive bias to the 'OFF' state or by a negative bias to the 'ON' state. (inset) Polarity of switching is usually controlled by the asymmetry of the interfaces as fabricated; for all reported devices the top interface is Schottky-like and the bottom interface is ohmic-like. (b) and (c) 50 cycles of the bipolar switching for a 50 × 50 nm^2 nano-device and a 5 × 5 μm^2 micro-device. Of note, both devices are switched ON by a negative bias and OFF by a positive bias on the top electrodes. The variances of ON switching voltage (V_{ON}) and OFF switching current (I_{OFF}) are larger for the micro-device. The ON/OFF conductance ratios are ~10^3 for both devices; the current level of the nano-device is ~100× smaller; the area of the nano-device is ~10^4 smaller. (d) AFM image of 1 × 17 nano-junctions. The cross-section profile shows 50 nm half pitch and 13 nm height nanowires. The 2nd and 15th junctions (indicated by blue arrows) were electrically formed 'ON', and do not show any detectable deformation. (e) AFM image of a 5 × 5 μm^2 junction before electrical forming. The cross-section profile shows about 5 μm width and 30 nm height of the top electrode (TE). (f) AFM image of the same micron junction after a negative bias forming process. Remarkably, a 1 μm × 50 nm bubble has formed along the edge of the bottom electrode (BE). A distinct pointed tip suggests gas eruption.

melting, solid electrolysis, and others [34–43]. Electro-reduction has been shown in bulk oxide materials under electric bias [9, 44, 45]. The physical deformation behavior in our devices shows a strong dependence on bias polarity and junction size. We test these dependences to establish oxygen ion and oxygen vacancy creation via electro-reduction of the TiO_2 as the core mechanism behind the physical deformation and electrical conductivity changes during electroforming.

In our Pt/TiO_2/Pt crosspoint junctions, the middle TiO_2 film is always a blanket layer across the wafer and the junction is defined by the overlapping area of the top and bottom electrodes (see also supplemental information figures S2, S3 (available at stacks.iop.org/Nano/20/215201)). We postulate the physical deformation occurs when negatively charged oxygen ions drift to the positively biased electrode (anode) and are discharged there to form O_2 gas, which accumulates to a certain pressure and then erupts from the mechanically weakest part of the thin films.

Why is no physical deformation observed in the nano-devices? The nano-devices are 100 times smaller in linear dimension and 10^4 times smaller in volume than the micro-devices (the TiO_2 film thickness is the same). Assuming that the oxide film is reduced to a certain degree when the device is electroformed, we see that the amount of material decomposition, gas produced, and pressure accumulated before deformation in a nanoscale device may be $\sim 10^4$ times smaller than for a micro-scale device. Amplifying this difference, diffusion of gas to escape at the electrode edges should also be $(100)^2 \approx 10^4$ times faster. Although a qualitatively similar switching behavior has been observed for both micro- and nano-junctions, the reproducibility of each switching loop in the nano-device is better than in the micro-device; voltage and current variances are lower (figures 1(b) and (c)). We attribute this improved performance to less physical disruption during the electroforming process.

In order to more clearly observe the gas bubble behavior under electric field, an even larger 60 μm device was tested (figure 2). In such a large device, more gas is likely produced and it is more difficult ($\sim$100 times slower again compared to the 5 μm devices) for the gas to diffuse to the edge of the electrodes. The schematic inset to figure 2(a) shows the device configuration. Both the Pt bottom electrode and the TiO_2 layer are blanket films and the Pt top electrode defines the junction area. In figure 2(b), -4 V applied to the top electrode (TE) induced a few bubbles, readily visible in the optical microscope images. The bubbles remain after removing the bias, as shown in figure 2(c). An opposite bias of $+4$ V leads to the shrinking of the previous bubbles, and the simultaneous formation of small new bubbles (figure 2(d)). The new bubbles grow in number and size in figure 2(e) when the positive voltage is maintained. After the removal of the $+4$ V, the bubbles shrink and disappear completely within seconds (figure 2(f)). Close inspection by AFM reveals remnant eruption-like features on the surface of the top electrode (figure 2(g)). A larger or longer applied voltage causes growth and agglomeration of bubbles, resulting in fewer, larger bubbles (figure 2(h)). Videos of the bubble evolution are available in the supplementary information (available at stacks.iop.org/Nano/20/215201).

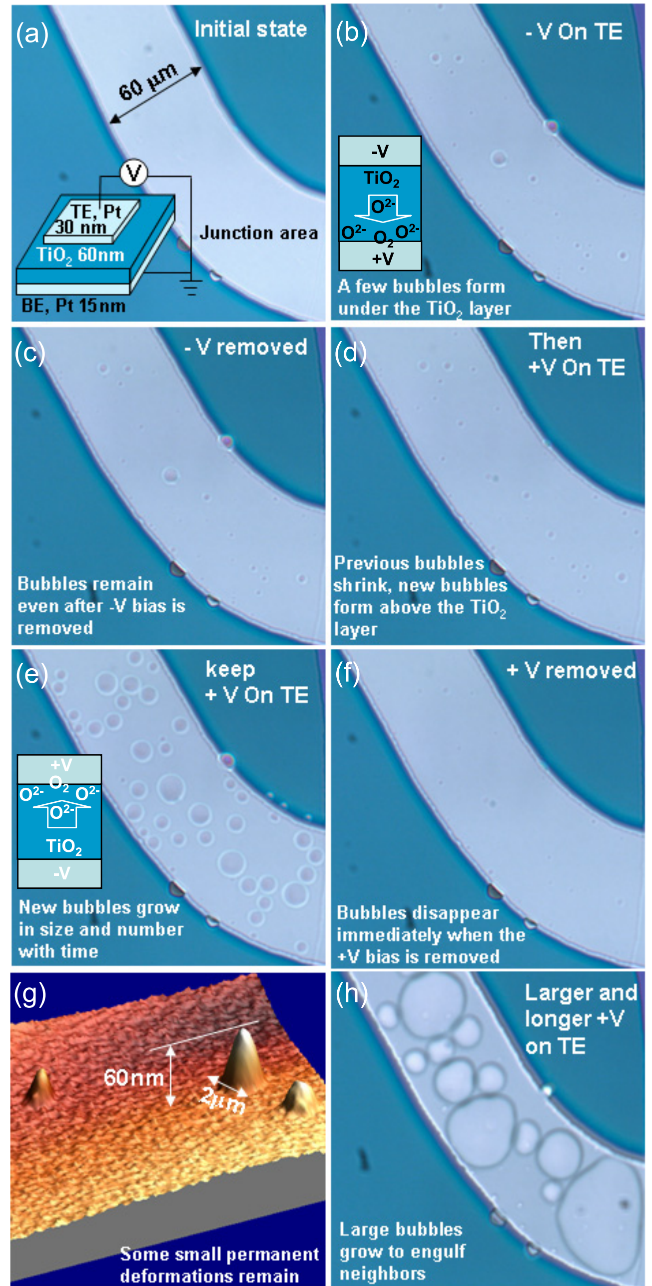

Figure 2. Gas bubble behavior under (b), (c) negative bias, then under (d)–(h) positive bias. (g) Atomic force micrograph of eruption features remaining after the bias voltage was removed. Videos of bubble evolution are available in the supplemental information (available at stacks.iop.org/Nano/20/215201).

In the case of a negative voltage on the top electrode, oxygen gas would form under the TiO_2 layer and be contained by the 60 nm TiO_2 and 30 nm Pt top electrode layers, illustrated schematically in figure 2(b). Conversely, with a positive voltage on the top electrode, gas would form above the TiO_2 and be contained only by the Pt electrode (schematic in figure 2(e)). We postulate that a higher gas pressure is needed to form a bubble under the TiO_2 (figure 2(b)), which leads to fewer and smaller gas bubbles compared to bubbling above the TiO_2 (figure 2(e)). The bubbles under the TiO_2

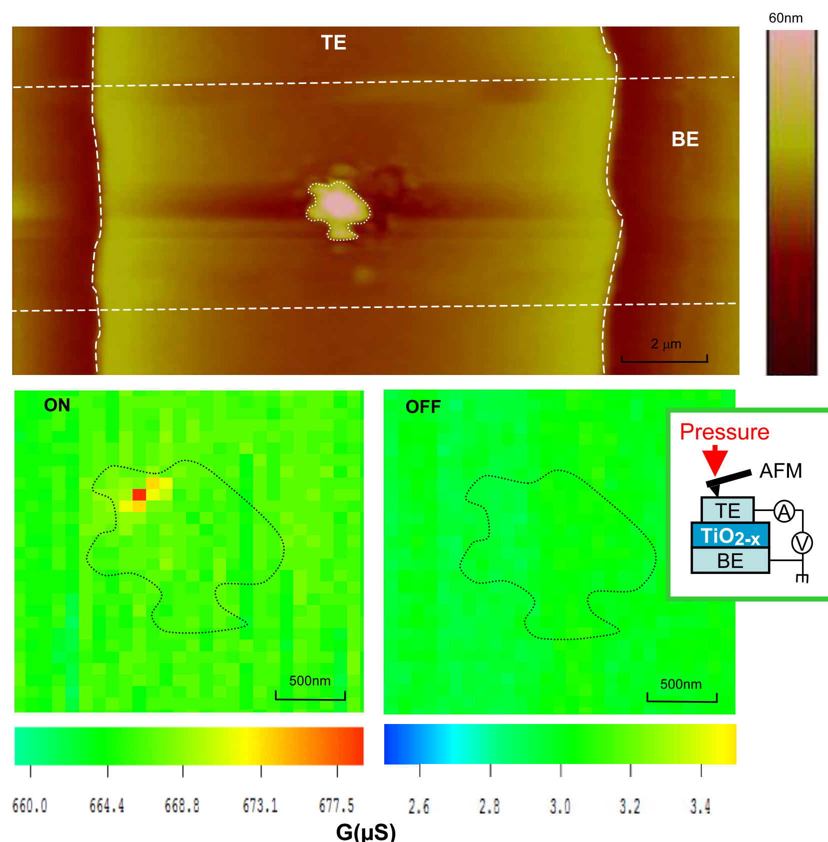

Figure 3. Conducting channel formation and dissolution adjacent to the bubble area, as observed with the local pressure-modulated conductance microscopy (LPCM) technique (schematic). Top, AFM image of a micron-size device with a bubble created in the center of the junction area during the forming step (negative bias on TE in this case). Dashed lines indicate the electrode edges. Left, LPCM conductance image of the bubble region in the low resistance state (LRS), where a conductance peak (in red) indicates the existence of a local conducting channel at the periphery of the bubble area. Right, after switching back to the high resistance state (HRS) the conducting channel disappears.

usually do not disappear until a positive voltage is applied (figure 2(d)), when the gas may be reincorporated into the film via electrochemical reaction. The gas formed above the TiO_2 film readily escapes at the top electrode edge or through small eruption features on the top electrode surface (figure 2(g)), so that no gas bubbles remain only a few seconds after removing the positive voltage. This scenario is further supported by delamination experiments in which $-$V electroforming usually creates a round hole through the TiO_2 layer while +V forming essentially leaves the TiO_2 layer intact but just causes some deformation in the top Pt layer (see supplemental information figure S3 (available at stacks.iop.org/Nano/20/215201), and also the insets to figures 4(a) and (b)).

Because the devices are unpassivated and measured in atmosphere, it could be argued that oxygen from the ambient may be interacting with the oxide [46] during formation in a similar manner to the device in reference [46]. Calcia-stabilized-zirconia sandwiched between two porous Pt electrodes has been used as an oxygen sensor and demonstrated to pump oxygen from air into the sandwich structure at elevated temperatures over 500 °C [47]. In order to exclude the role of oxygen from air in the current study, electroforming has been carried out *in situ* in a SEM chamber with a pressure of 7×10^{-6} Torr. Similar bubbles were observed after electroforming in vacuum (see supplemental information figure S4 (available at stacks.iop.org/Nano/20/215201)), suggesting that at least part if not all of the gas inside the bubbles is released from the oxide layer as a product of electro-reduction.

A clear spatial correlation between the oxygen bubbles and the electrical switching is demonstrated via the local pressure-modulated conductance microscopy (LPCM) technique [48], as shown in figure 3. An AFM image shows a bubble formed in the center of the junction area after a negative voltage electroforming process. The creation of oxygen gas is accompanied by the concomitant creation of oxygen vacancies (V_O) in the TiO_2, or more precisely the TiO_{2-x}. Such vacancies are known to dope the semiconducting TiO_2 to high conductivities [49]. With the LPCM technique (see [41] for details), a small ~50 mV bias is applied between the top and bottom electrodes and the current flowing is monitored while scanning an AFM tip in contact mode over the top electrode. The AFM is not electrically connected—it simply serves to apply local pressure. Previous experiments [48, 50, 51] have established that local strain induced by the AFM tip reduces the gap between the electrode and the tip of a conducting channel inside the oxide film, typically causing a slightly higher current to flow through the junction. When such a spatially localized current increase occurs during scanning, the position of the AFM tip reveals the location of the conducting channel(s). One such channel is found immediately adjacent to the bubble area

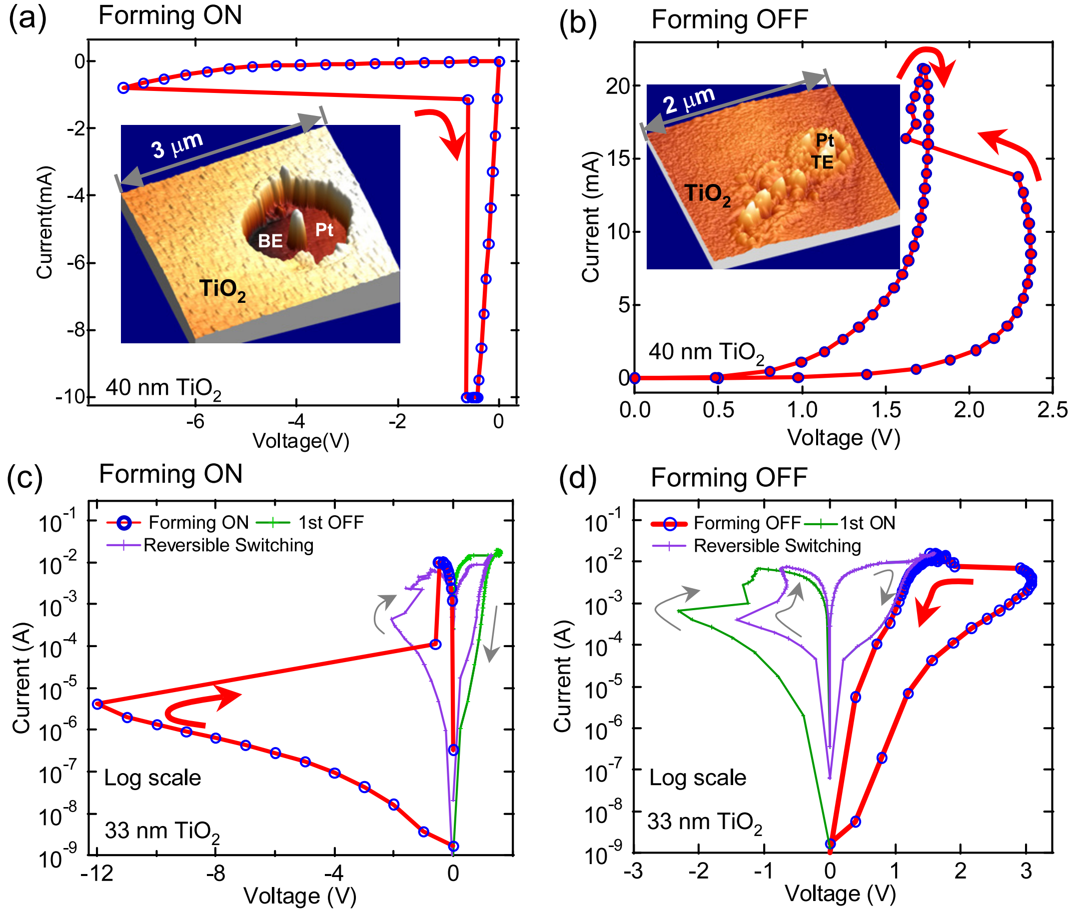

Figure 4. Electroforming results depend strongly on bias polarity and TiO_2 resistivity. (a), (b) Two devices from the same sample of 40 nm thick more conductive (120 Ω cm) TiO_2. Negative forming produces an ON state and requires high voltage but low current; positive forming yields the OFF state and requires lower voltage but higher current. Inset atomic force micrographs of the electroformed TiO_2 surface after the TE Pt layers were removed by delamination. $-V$ electroforming yielded a micron-size hole through the entire TiO_2 layer; in $+V$ electroforming the TiO_2 film is intact with minor TE Pt layer residue. (c), (d), Two devices from a second sample of thinner (33 nm) but more resistive (2300 Ω cm) TiO_2, as evidenced by lower virgin-state currents. A significantly higher electric field is required for both negative and positive forming. The first switching (ON or OFF) after forming is shown in green. Subsequent reversible switchings are shown in purple. All the devices ((a)–(d)) are engineered to have more oxygen vacancies at the bottom electrode/TiO_2 interface, defining a switching polarity of ON for $-V$ and OFF for $+V$ on the top electrode.

in the low resistance state. This conduction channel vanishes when the device is switched back to the high resistance state.

From the observations of figures 1–3, we conclude that the electroformation in the metal/oxide/metal devices is an electro-reduction process that creates localized, high conductance channels of oxygen vacancies through the oxide film. Oxygen gas forms at the anode, where oxygen ions are attracted and discharged. However, the oxygen ions and vacancies are likely created wherever in the junction there is a high electric field and resistance. The switching junctions studied are typically quite asymmetric [2], consisting of a more conductive ohmic-like interface (the bottom interface for our devices) and a more resistive Schottky-like interface (the top interface for our devices) (see figure 1(a) inset). We next investigate the polarity dependence of the electroforming process to reveal the role of electric field and electrical heating.

Opposite polarity electroforming produces different final junction states, as shown in figure 4 (see also figure 1(a)). Two devices from the same sample (40 nm TiO_2 with a resistivity of 120 Ω cm) are formed by either a negative voltage to the ON state (figure 4(a)) or a positive voltage to the OFF state (figure 4(b)). The forming process is typically too fast to be recorded and only a jump between two data points (before and after forming) is seen in the I–V curves with a voltage sweep. The voltage value just before the jump is defined as the electroforming voltage in this study. Importantly, the field strength for these two cases is very different. As shown in figures 4(a) and (b), positive voltage (+2.3 V) forming apparently requires a much smaller (∼ one third) average electric field compared to negative voltage forming (−7.8 V). The asymmetry of the two metal/oxide interfaces becomes critical here—the current level is much higher for positive voltages (the Schottky-like interface is forward-biased), meaning a larger electrical Joule heating effect is possible. Independent experiments suggest self-heating of several hundred degrees may be possible in these devices [52]. Oxygen vacancy mobility increases by about seven orders of magnitude from room temperature to 240 °C, as estimated by

combining the Arrhenius law for the temperature dependence of diffusion and the Nernst–Einstein relation. Electroforming is not purely a heating effect, however, since it is highly polarity dependent and annealing the TiO_2 without bias did not produce gas bubbles (see supplemental information figure S5 (available at stacks.iop.org/Nano/20/215201)). Instead, an electroforming process triggered by high electric field and enhanced by electrical heating, where oxygen ions (vacancies) are created in the region of high field and then drift towards the anode (cathode), is most consistent with these data.

In this process, a negative voltage on the top electrode produces a large voltage drop at the reverse-biased Schottky-like top interface (figure 4(a)). Positively charged oxygen vacancies would likely be produced here and stay at the top interface until their doping effect reduces the electronic barrier to a conductive, and hence low electric field, state. Junction currents will then increase and be limited by the insulating bulk film, now the high electric field region of the device. Creation and drift of more V_Os across the bulk film quickly creates a conducting channel and low resistance ON state where *both* the resistive bulk film and resistive Schottky-like interface have been penetrated by a conducting channel. The devices were further examined after removing the top electrode layer with a delamination technique [53]. A round hole in the oxide layer is usually observed (inset to figure 4(a)) after electroforming with a negative voltage, indicating the O_2 gas bubbles likely formed under the oxide layer to weaken the bottom electrode/oxide interface (more delamination results are shown in the supplemental information, figure S3 (available at stacks.iop.org/Nano/20/215201)).

In the case of a positive voltage on the top electrode, the forward-biased Schottky-like top interface is relatively conductive and the voltage drop is instead concentrated across the bulk film. The O^{2-} anions would drift toward the positively biased top electrode and discharge there to form O_2 gas on top of the TiO_2 layer but under the electrode. Oxygen vacancies would drift via high diffusion paths (e.g. defects, grain boundaries) away from the top interface towards the bottom electrode to form conducting channels through the oxide film. The electric field polarity repels the growing vacancy channels from touching the top electrode—the Schottky-like barrier is not heavily reduced after forming and the post-forming state is OFF. In other words, the conducting channel penetrates the bulk film but *not* the Schottky-like interface region. In addition, the TiO_2 layer is much less physically deformed by gas bubbling and eruption, since the O_2 has formed on top of the TiO_2 film. The inset in figure 4(b) shows that the TiO_2 is essentially intact after delaminating the top Pt, indicating the deformation has preferentially weakened the oxide/top electrode interface in this case.

This model of vacancy creation and drift is supported by the electroforming and subsequent switching I–Vs of devices with a thinner (33 nm) but more resistive (2300 Ω cm) oxide layer (figures 4(c) and (d)). These devices exhibit similar behavior to the previous 40 nm oxide devices. Different from some device structures where the forming voltage increases proportionally with the oxide thickness [54], an even larger voltage (−12 or +3 V) or electric field is required to form these thinner devices. This can be rationalized by considering the possible enhancement from Joule heating, which could yield a several hundred degree temperature increase [52] for these thicker but more conductive and thus higher current devices (figures 4(a) and (b)).

The electroforming process with bubble formation is potentially destructive and certainly difficult to control. Technologically, it is essential to eliminate this device variance for computer circuit applications. We have postulated that electroforming by either positive or negative voltage creates a conductance channel(s) though the bulk oxide film, and subsequent ON/OFF switching is concentrated at one or both interface regions. One approach to engineer a device that obviates electroforming is to thin the oxide film, eliminate the 'bulk' region and just keep the 'switching interface'. Figure 5 shows I–V data from such a device. The TiO_2 for this device is only 4 nm thick and the I–V curve for the initial electroforming step (red) is essentially identical to the I–Vs of subsequent reversible ON switching (purple). Significantly, the resistances for both ON and OFF states are comparable to the previous devices with the thick TiO_2 layers—supporting the postulate that electroforming primarily creates conductance channels across the bulk oxide film. However, the device with a 4 nm oxide exhibits an increasing conductance in both ON and OFF states with switching cycling (see figure S7 (available at stacks.iop.org/Nano/20/215201)), probably due to the lack of an oxygen reservoir for the reversible migration of oxygen ions and vacancies. To solve this problem and also further verify the electroforming mechanism, we added a highly reduced, i.e. conductive, but thick (120 nm) TiO_{2-x} layer to otherwise identical 4 nm TiO_2 devices during the fabrication process and found that the electroforming process in this new device with thick oxide is also eliminated and no distinct trend of the resistance drift is observed during the 200 cycles, as shown in figure 5(b). This again supports the postulate that if conductance channels are somehow created in the bulk oxide during the fabrication process, no further electroforming is required, which could be the cause of some electroforming-free devices [55]. Various thicknesses of the oxide layer have been studied and a qualitatively similar switching behavior (shown in figure 1) has been observed with the oxide thickness between about 15–60 nm. No distinct forming process is required when the oxide is thinner than about 6 nm, but tunneling and hot-spot issues become severe when the oxide thickness is less than 3 nm.

In summary, we have demonstrated that electroforming of metal/oxide/metal switches is an electro-reduction and drift process triggered by high electric fields and enhanced by electrical Joule heating. Oxygen vacancies are created and drift towards the cathode forming localized conducting channels in the oxide film. Simultaneously, O^{2-} ions drift towards the anode and are discharged there, evolving O_2 gas and causing physical deformation of the junction. The gas eruption, physical deformation and electroformation are bias polarity dependent. The switching polarity of the junction is usually dominated by the as-fabricated asymmetry of the two interfaces and thus remains independent of the forming bias polarity. The problematic physical deformation can be

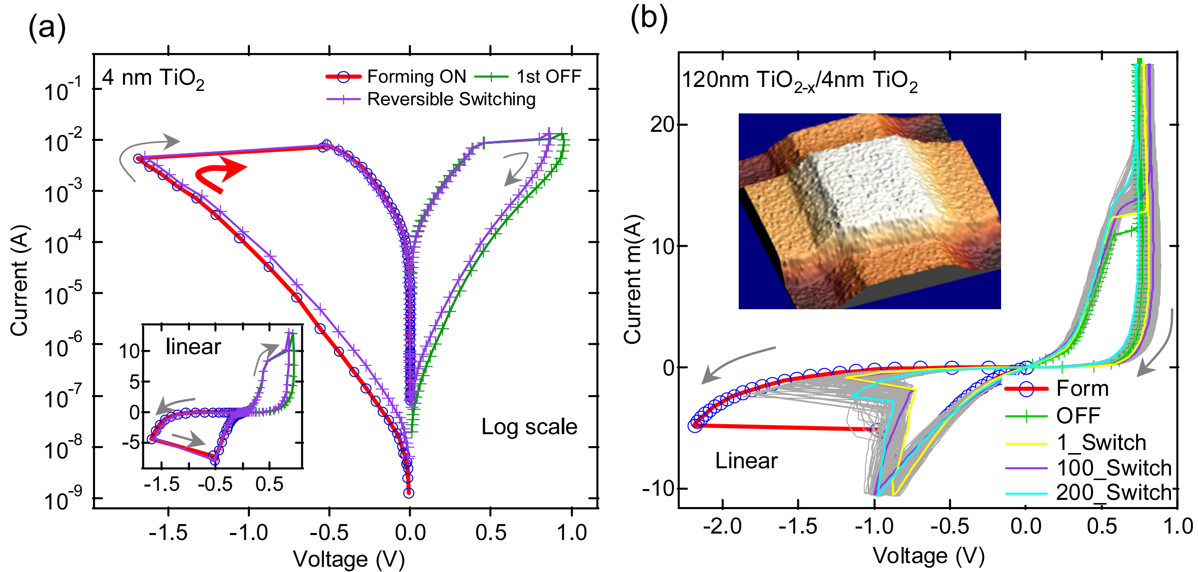

Figure 5. Engineering the device to eliminate the need for electroforming. Thinning the TiO_2 insulator to 4 nm and just keeping the key electrode/TiO_2 'switching interface' reveals that the electroforming is primarily a process of creating conductance channels across the bulk insulator. (a), A Pt/4 nm TiO_2/Pt device. The forming I–V (red) is essentially identical to the subsequent ON switching I–V (purple). The shape and amplitude of conductance switching is comparable to those devices with much thicker TiO_2 layers. (b), The data from a Pt/120 nm TiO_{2-x}/4 nm TiO_2/Pt device, showing 200 consecutive switching loops after the forming step. The thick TiO_{2-x} is already highly reduced during device fabrication and thus no electroforming is needed; the key interface is again the electrode/TiO_2. Neither sample a nor b show detectable physical deformation by AFM.

reduced to an undetectable level by shrinking the junction size to the nanoscale. More importantly, the forming process can be essentially eliminated by restricting the insulating TiO_2 oxide to a very thin $\sim$ few nanometer layer, alone or in combination with thick but conductive oxide layers. Environmental oxygen interaction may reduce the long term device reliability without careful packaging. These results should be applicable to all resistive and memristive oxide switch devices, and are likely extensible to other oxides in common use as electronic materials, including semiconductor oxides in CMOS, DRAM and flash devices.

References

[1] Strukov D B, Snider G S, Stewart D R and Williams R S 2008 *Nature* **453** 80–3
[2] Yang J J, Pickett M D, Li X, Ohlberg D A A, Stewart D R and Williams R S 2008 *Nat. Nanotechnol.* **3** 429–33
[3] Chua L O 1971 *IEEE Trans. Circuit Theory* **18** 507–19
[4] Hickmott M T 1962 *J. Appl. Phys.* **33** 2669–82
[5] Sawa A, Fujii T, Kawasaki M and Tokura Y 2004 *Appl. Phys. Lett.* **85** 4073
[6] Liu S Q, Wu N J and Ignatiev A 2000 *Appl. Phys. Lett.* **76** 2749–51
[7] Chen X, Wu N, Strozier J and Ignatiev A 2006 *Appl. Phys. Lett.* **89** 063507
[8] Watanabe Y *et al* 2001 *Appl. Phys. Lett.* **78** 3738–40
[9] Szot K *et al* 2006 *Nat. Mater.* **5** 312–20
[10] Beck A, Bednorz J G, Gerber C, Rossel C and Widmer D 2000 *Appl. Phys. Lett.* **77** 139
[11] Jeong D S, Schroeder H and Waser R 2007 *Electrochem. Solid State Lett.* **10** G51–3
[12] Wu J, Mobley K and McCreery R 2007 *J. Chem. Phys.* **126** 24704
[13] Jameson J R *et al* 2007 *Appl. Phys. Lett.* **91** 112101
[14] McGovern W R, Anariba F and McCreery R 2005 *J. Electrochem. Soc.* **152** E176
[15] Seo S *et al* 2004 *Appl. Phys. Lett.* **85** 5655
[16] Kozicki M N, Park M and Mitkova M 2005 *IEEE Trans. Nanotechnol.* **4** 331–8
[17] Terabe K, Hasegawa T, Nakayama T and Aono M 2005 *Nature* **433** 47–50
[18] Waser R and Aono M 2007 *Nat. Mater.* **6** 833–40
[19] Watanabe Y, Bednorz J G, Bietsch A, Gerber Ch, Widmer D, Beck A and Wind S J 2001 *Appl. Phys. Lett.* **78** 3738–40
[20] Waser R 2005 *Nanoelectronics and Information Technology* (Weinheim: Wiley-VCH)
[21] Meijer G I 2008 *Science* **319** 1625–6
[22] Rozenberg M J, Inoue I H and Sanchez M J 2006 *Appl. Phys. Lett.* **88** 033510
[23] Chen A, Haddad S, Wu Y C, Fang T N, Kaza S and Lan Z 2008 *Appl. Phys. Lett.* **92** 013503
[24] Mead C 1989 *Analog VLSI and Neural Systems* (Reading, MA: Addison-Wesley)
[25] Boahen K 2005 *Sci. Am.* **292** 56–63
[26] Snider G S 2008 *IEEE Int. Symp. Nanoscale Architecture* pp 85–92
[27] Dearnaley G, Stoneham A M and Morgan D V 1970 *Rep. Prog. Phys.* **33** 1129–91
[28] Chudnovskii F A, Odynets L L, Pergament A L and Stefanovich G B 1996 *J. Solid State Chem.* **122** 95–9

[29] Odagawa A, Katoh Y, Kanzawa Y, Wei Z, Mikawa T, Muraoka S and Takagi T 2007 *Appl. Phys. Lett.* **91** 133503
[30] Janousch M, Meijer G I, Staub U, Delley B, Karg S F and Andreasson B P 2007 *Adv. Mater.* **19** 2232–5
[31] Horcas I, Fernandez R, Gomez-Rodriguez J M, Colchero J, Gomez-Herrero J and Baro A M 2007 *Rev. Sci. Instrum.* **78** 013705
[32] Jung G Y, Ganapathiappan S, Ohlberg D A A, Olynick D L, Chen Y, Tong W M and Williams R S 2004 *Nano Lett.* **4** 1225–9
[33] Jung G Y *et al* 2006 *Nano Lett.* **6** 351–4
[34] Dearnaley G, Morgan D V and Stoneham A M 1970 *J. Non-Cryst. Solids* **4** 593–612
[35] Park K C and Basaviah S 1970 *J. Non-Cryst. Solids* **2** 284–91
[36] Emmer I 1974 *Thin Solid Films* **20** 43–52
[37] Schroeder H and Jeong D S 2007 *Microelectron. Eng.* **84** 1982–5
[38] Sharpe R G and Palmer R E 1996 *J. Phys.: Condens. Matter* **8** 329–38
[39] Blessing R, Pagnia H and Sotnik N 1981 *Thin Solid Films* **85** 119–28
[40] Rakhshani A E, Hogarth C A and Abidi A A 1976 *J. Non-Cryst. Solids* **20** 25–42
[41] Vekderber R R, Simmons J G and Eales B 1967 *Phil. Mag.* **16** 1049
[42] Szot K, Dittmann R, Speier W and Waser R 2007 *Phys. Status Solidi (RRL)* **1** R86–8
[43] Jeong D S, Schroeder H, Breuer U and Waser R 2008 *J. Appl. Phys.* **104** 123716
[44] Szot K, Speier W and Eberhardt W 1992 *Appl. Phys. Lett.* **60** 1190
[45] Chen G Z, Fray D J and Farthing T W 2000 *Nature* **407** 361–4
[46] Verbakel F, Meskers S C J and Janssen R A J 2006 *Appl. Phys Lett.* **89** 102103
[47] Graham J A 1984 Purification of mercuric iodide and related semiconductor processing topics *PhD Thesis*
[48] Lau C N, Stewart D R, Williams R S and Bockrath M 2004 *Nano Lett.* **4** 569–72
[49] Knauth P and Tuller H L 1999 *J. Appl. Phys.* **85** 897–902
[50] Lau C N, Stewart D R, Bockrath M and Williams R S 2005 *Appl. Phys.* A **80** 1373–8
[51] Miao F, Ohlberg D, Stewart D R, Williams R S and Lau C N 2008 *Phys. Rev. Lett.* **101** 016802
[52] Borghetti J L *et al* 2009 Electrical characterization of the internal states of electroformed titanium dioxide memristive switches, unpublished
[53] Blackstock J J *et al* 2008 *J. Am. Chem. Soc.* **130** 4041–7
[54] Verbakel F *et al* 2007 *Appl. Phys. Lett.* **91** 192103
[55] Verbakel F, Meskers S C J, Leeuw D M de and Janssen R A J 2008 *J. Phys. Chem.* C **112** 5254–7